Composite Structures 367 (2025) 119228

Contents lists available at ScienceDirect

Composite Structures

journal homepage: www.elsevier.com/locate/compstruct

A simplified fatigue characterization of defective CFRP laminates with infrared thermography

José Vicente Calvo *, Norberto Feito, Eugenio Giner

Institute of Mechanical and Biomechanical Engineering – I2MB, Department of Mechanical and Materials Engineering, Universitat Politècnica de València, Camino de Vera s/n, 46022 Valencia, Spain

A R T I C L E I N F O

Keywords:
CFRP
Fatigue
Thermography
Out-of-plane waviness

A B S T R A C T

Fiber misalignment and out-of-plane waviness are defects encountered in composite material laminates. These defects are particularly prone to occur when adapting the laminate to angular or complex geometries. Using these defective laminates in aerospace applications can undermine their structural integrity and impact their mechanical properties. This work involves a study of applying infrared thermography techniques to estimate the fatigue limit based on the energy dissipated during tensile testing. Defect-free CFRP laminates and laminates with several out-of-plane waviness distributed along the sample and through the thickness are tested at various stress levels. Estimation of their fatigue limit using thermography is performed, and the results show a significant agreement to those obtained through *S-N* curves, with less than 2% error for defect-free specimens and 13% for defective ones. A reduction in mechanical properties and service life is observed in the material with defects compared to defect-free material, with a decrease of 16% of the ultimate strength and 40% of the fatigue limit. The study supports the application of thermography as a simple and rapid technique to detect and locate this type of defect and characterize the fatigue limit of the CFRP laminate.

1. Introduction

In the current aerospace and energy industries, carbon fiber-reinforced polymer laminates (CFRP) are widely used due to their favorable combination of mechanical properties, such as high specific strength and stiffness, low density, and the ability to withstand adverse environmental conditions. However, defects that occur during the manufacturing of laminates, such as fiber misalignment or out-of-plane waviness, can compromise their structural integrity and reduce their service life [1,2].

Manufacturing defect-free composite materials is challenging due to process-induced distortions, which result in geometric variations from the mold shape and lead to defects such as voids, fiber waviness, and porosity [3]. These defects are influenced by factors like mold features, material characteristics, and bagging practices [4]. For example, fiber mismatch, particularly in curved sections, further exacerbates the formation of wavy regions [5–7]. Temperature gradients can also cause residual stresses due to differences in thermal expansion between the fiber and matrix, leading to fiber waviness [8]. Even the new advanced composite manufacturing techniques, such as the automated fiber placement, can have manufacturing defects caused by fiber path imperfections generating local non-uniform consolidation [9,10]. With the intention of mitigating these manufacturing defects, several authors have proposed guidelines and numerical tools in this field [9,11].

To date, published works have demonstrated that out-of-plane waviness in CFRP laminates significantly reduces their strength and fatigue life. In the 90s, different works analyzed the influence of the waviness in stiffness and ultimate strength of the lamina from an analytical point [12–14]. In the last ten years, several studies have been published in the field [15–17]. These works represent an advance in knowledge for predicting and understanding the influence of the different parameters of the waviness (amplitude δ, wavelength λ, and maximum deflection angle θ) on the severity of the defect and its influence on the mechanical behavior.

In the last decades, the use of finite element modeling for simulating a more realistic defect has increased. For example, Mukhopadhyay et al. [18] analyzed the effect of waviness with varying stacking sequences in quasi-isotropic CFRP laminates. Results proved that these defects act as local stress concentrators, reducing the tensile strength of the laminate by 23%. In a later study, [19], the same authors concluded that fiber misalignment decreases the material fatigue strength using finite element models. The FEM implementation has been used to simulate the

* Corresponding author.
E-mail address: jocalor@upv.es (J.V. Calvo).

https://doi.org/10.1016/j.compstruct.2025.119228
Received 3 December 2024; Received in revised form 22 February 2025; Accepted 25 April 2025
Available online 28 April 2025

fatigue damage [20] and the damage initiation [21]. The authors of these works concluded that the fatigue life of wrinkled specimens is approximately an order of magnitude lower than that of pristine specimens for a given load and severity. These studies emphasize the importance of detecting and characterizing such defects in CFRP laminates. However, they also point out a limitation of this approach: it is restricted to ply-by-ply modeling, making component-scale models computationally expensive [22]. To advance this line of knowledge, the development and application of non-destructive techniques, such as thermal sensors or acoustic measurements, are presented as useful tools for defect detection and quantification.

In the specific case of using thermographic sensors for predicting the fatigue life of CFRP components, some studies in the literature have demonstrated the utility of this technique and its application in characterizing the material fatigue life. For instance, Toubal et al. [23] studied the application of infrared thermography in woven CFRP laminates subjected to cyclic tensile loads, establishing a relationship between the average surface temperature surrounding an open hole and the evolution of accumulated damage in the laminate for mechanical property degradation models. Feito et al. [24] applied thermography to thick CFRP multi-directional laminates with drilled holes and the increase in temperature was double in defective areas compared to defect-free areas. It was demonstrated that an out-of-plane wave in the laminate could work as a stress concentrator with greater influence than a small, drilled hole, and therefore, conditioning the location of the material failure. Risitano et al. [25,26] developed a methodology for determining the fatigue limit and obtaining the *S-N* curves for steels, reducing the time for testing considerably, and obtaining results with an error of less than 10%. Colombo et al. [27] applied the Risitano's methodology to composite laminates, specifically GFRP, and compared the predictions with those obtained using traditional methods, achieving a strong agreement between the two approaches. Later, Montesano et al. [28] introduced a slight modification of the formulation and demonstrated the possibility of using it with woven CFRP laminates, obtaining an excellent agreement with the experimental data. Huang et al. [29] advanced with this methodology including mechanisms of fatigue damage evolution and proved that the new formulation estimates the fatigue life of woven and unidirectional CFRP defect-free laminates using thermographic techniques. This model was subsequently applied to fiberglass laminates with out-of-plane waviness [30], yielding good results in defect localization and fatigue limit estimation, making it one of the few studies to date conducted on long fiber-reinforced polymer materials (LFRP) with out-of-plane waviness defects using this thermographic methodology. Recent investigations, such as the work by An et al. [31] have revealed that certain models exhibit limitations when applied to low-cycle conditions in pristine CFRP composites. These findings underscore the necessity of further research to enhance the understanding and development of these models.

This study explores the application of infrared thermography to CFRP laminates containing multiple out-of-plane waviness defects located at varying depths through the thickness simultaneously—a scenario scarcely addressed in the literature. While most existing studies focus on pristine specimens, this work investigates laminates with imperfections, offering insights into the behavior of materials under practical conditions. The technique is used not only to detect and locate these defects but also to predict the fatigue limit based on temperature variations during cyclic tensile testing. Furthermore, this study explores the validation of existing thermographic models in the context of defective laminates, an area that has been scarcely explored. Laminates with and without defects are tested to derive *S-N* curves, and results are compared with predictions from various thermographic methods. The findings demonstrate that thermography enables accurate fatigue limit estimation, regardless of the reduction in properties caused by defects. This highlights its potential as a transformative tool for enhancing the structural integrity of critical structures while significantly reducing testing costs and time. By addressing the challenges posed by defective laminates, this study provides a novel approach to the application of thermography in fatigue analysis, offering a practical and advanced contribution to the field.

2. Materials

The manufacturing of the specimens was carried out by the company Titania S.L. (Puerto de Santa María, Spain). The CFRP laminate consists of 22 unidirectional prepreg plies provided by Hexcel Corporation (Stamford, USA). Each ply contains a carbon fiber volume fraction of 59.2% of type IMA-12K. This laminate, representative of the aerospace industry, has been stacked following the sequence $[45/0/\text{-}45/90/0/90/0/90/\text{-}45/0/45]_s$. The dimensions of each specimen are $200 \times 15 \times 4.1$ mm, as shown in Fig. 1. Fiberglass tabs of PREPREG CYCOM 7701-38-G7781-296-1000, 45 mm in length, have been added at the ends.

Two distinct batches of specimens were prepared: one batch was defect-free, while the other included inserts of the same material placed in the transverse direction to induce multiple out-of-plane waviness during the manufacturing process. In this batch with defects, 7 inserts were introduced, spaced 20 mm apart, along the loading direction (direction 1), with the first insert positioned 35 mm from one end, as illustrated in Fig. 2. The position of the inserts along the thickness varies in height but they are located symmetrically with respect to the central wave. The central insert is positioned beneath the first 2 plies, the next inserts are under 7 plies, the subsequent ones are placed under 13 plies, and the end inserts are under 18. Due to this distribution, the undulation at one end is fully covered by the tabs, while at the other end, it is only partially covered.

All generated waviness defects have been geometrically characterized, resulting in a length of 9.6 ± 1 mm, a maximum height of 0.5 ± 0.04 mm, and an inclination of $6.8 \pm 1.3^\circ$. For this characterization, the Nikon SMZ745T stereomicroscope was used with its zoom range from $0.67\times$ to $5\times$ to examine samples in detail. Fig. 3 shows an image of a central waviness defect, captured with an optical magnifying glass, indicating the three geometric parameters.

3. Experimental methodology

Tests were conducted using an INSTRON 8801 hydraulic testing machine with a 100 kN load cell. The specimens from each batch were divided into three groups. The first group was dedicated to quasi-static tests to obtain the ultimate tensile load of the laminate. The second group underwent fatigue tests to acquire the *S-N* curve. The last group was used for the thermography-based fatigue limit estimation. This group was subjected to fatigue tests in blocks of 7000 cycles, increasing the load between blocks and allowing the specimen to cool until it reached room temperature again. All fatigue tests were performed in tension, load-controlled, with $R = 0$ and a frequency of 5 Hz.

A FOTRIC 348A camera (Dallas, USA) was used for capturing thermal images. During the tests, a reference specimen was placed alongside the loaded specimen. This specimen was free (unloaded), so the evolution of the room temperature is captured in this sample. This information will be used subsequently to eliminate the influence of ambient temperature variation in the sample tested. The setup is illustrated in Fig. 4. The thermal images were processed with the software AnalyzIR.

The procedure used with the last group follows Huang's methodology [29]. In that study, the method was used in defect-free CFRP laminates, but the present study examines this strategy with laminates in the presence of out-of-plane defects. This methodology is based on the relationship between energy dissipation and the stress level of the specimen. The objective is to identify the threshold at which energy dissipation indicates that the specimen has entered a load regime where damage initiates, leading to eventual fatigue failure. This threshold, commonly referred to as the fatigue limit, is typically defined at $2\cdot10^6$ cycles. Below this load level, the specimen can be considered to have an infinite life [32] as shown in the diagram of Fig. 5.

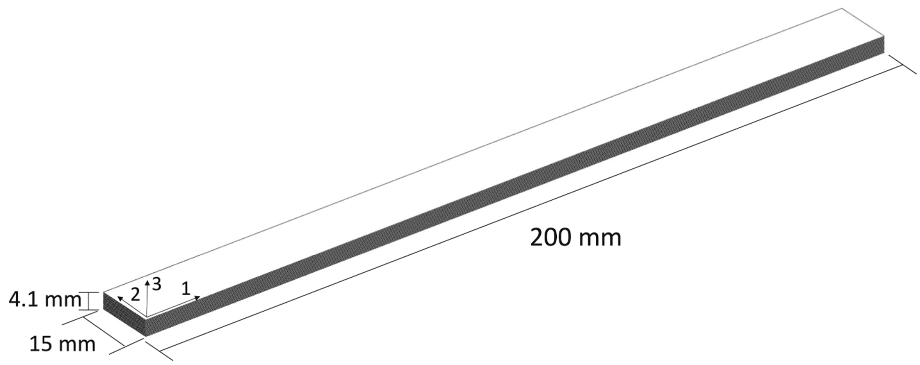

Fig. 1. Dimensions of defect-free specimens.

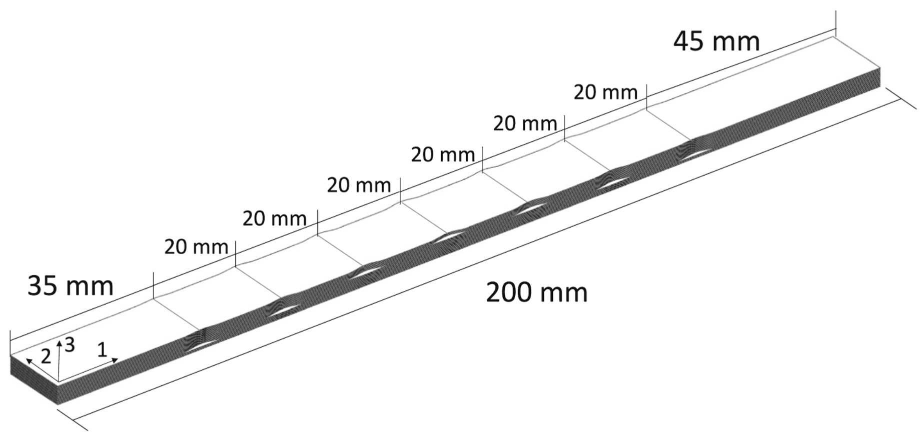

Fig. 2. Dimensions of specimens with defects.

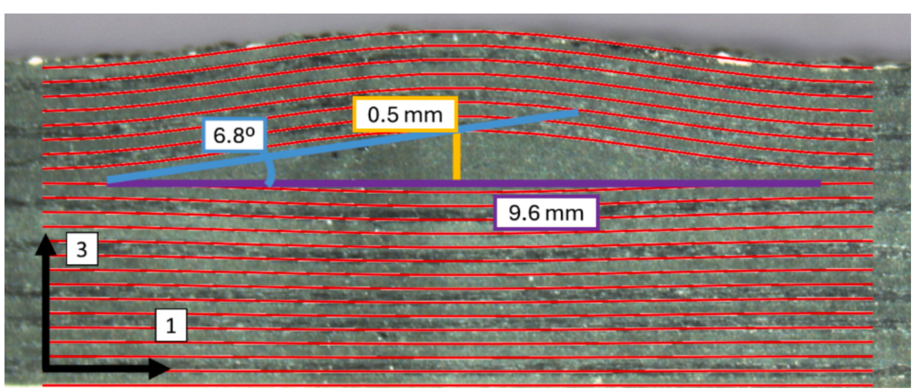

Fig. 3. Geometric characterization of one of the introduced defects.

From Huang [29], the local heat conduction equation can be used for linking the energy dissipated with the temperature [33–35] following Eq. (1), where ρ is the mass density, C is the heat capacity, and k the heat conduction coefficient. All of them are considered constant and independent.

$$\rho \cdot C \cdot \dot{T} - \mathrm{div}(k \cdot \nabla T) = d_i + s_{the} + s_{ic} + r_e \tag{1}$$

where T is the temperature. On the left side of the equation, the first term is the heat storage rate due to temperature change; the second is the heat loss by conduction. The right side of the equation represents the heat sources: d_i, s_{the}, s_{ic}, and r_e are the intrinsic dissipation source, the thermoelastic source, the heat source induced by coupling between internal variables (due to changes in the microstructure) and temperature, and the external heat supply, respectively. The thermoelastic and the internal coupling sources can be neglected under uniform uniaxial loading [36,37]. External heat can be eliminated by using a reference specimen placed nearby to keep track of any room temperature change and subtracting it.

If the intrinsic energy dissipation d_i remains unchanged the temperature will increase up to a certain value, where the heat storage and the heat loss reach an equilibrium with the intrinsic energy dissipation. As illustrated in Fig. 6, various studies have demonstrated that the testing process of a specimen involves three distinct phases leading up to the final fracture [25,26,28,35,38]. In Stage 1, the temperature increases from room temperature. During Stage 2, the temperature remains stable for the longest period. Stage 3 experiences a sharp increase just before final failure. This indicates that the intrinsic energy

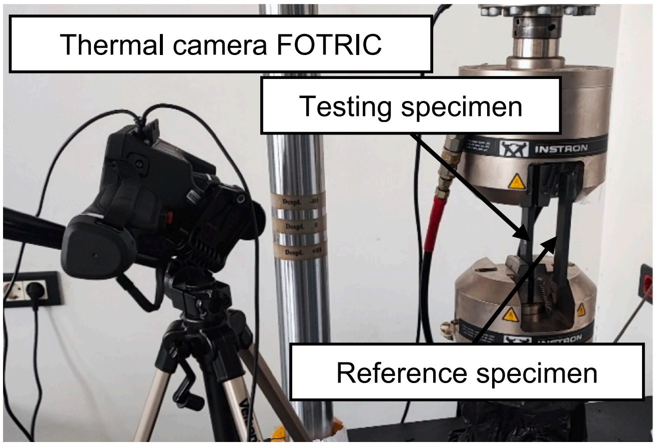

Fig. 4. Experimental setup.

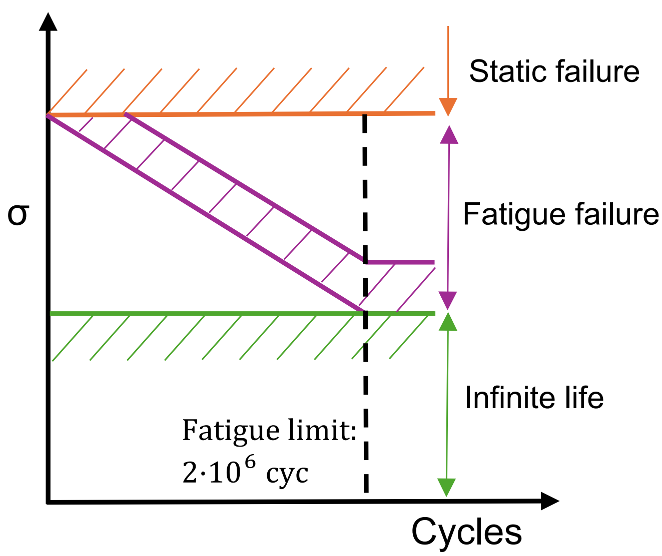

Fig. 5. Fatigue life diagram.

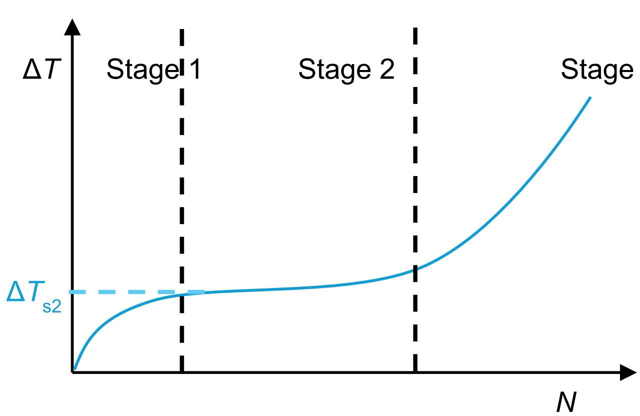

Fig. 6. Temperature evolution in a dynamic test.

dissipation remains constant in Stage 2, meaning a stable rate of damage accumulation during this phase.

Different applied loading stresses result in different stabilized temperatures, allowing a relationship between stabilized temperature and applied stress. Once all these points are plotted, two linear regressions define this relationship. As depicted in Fig. 7, the intersection of the lines

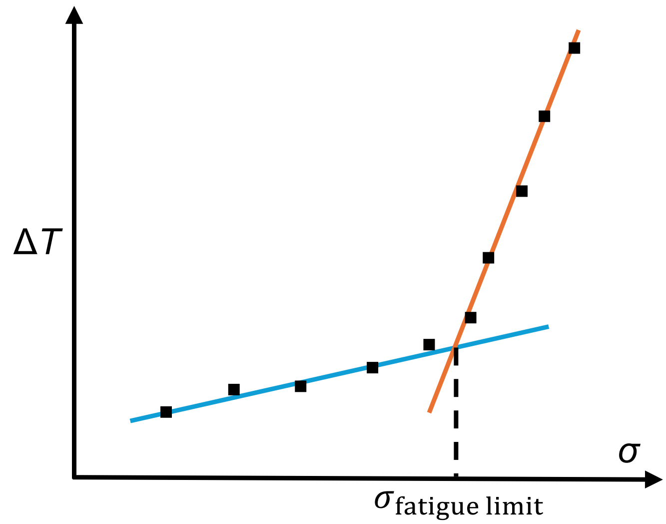

Fig. 7. Fatigue limit determination through thermographic methodology.

represents the fatigue limit [39,40]. This methodology provides a rapid method for characterizing the fatigue limit, which is a significant advantage over the costly traditional methods. This is because it is not necessary to reach fatigue failure to obtain these values.

Among the methods developed by Huang et al. [37] to locate this point, in this work we apply the technique based on R^2. This technique involves performing all possible combinations with the points (Applied Stress – Steady Temperature Increase) to obtain two intersecting lines through linear regression. The R^2 of every combination is calculated, and the pair with the highest R^2 values is selected for the fatigue limit estimation [37].

From this relationship, the ΔT can be defined as a function of the applied stress through piecewise linear functions:

$$\Delta T = \mathrm{f}(\sigma) = \begin{cases} m_1\cdot\sigma + b_1 & (\sigma < \sigma_{\text{fatigue limit}}) \\ m_2\cdot\sigma + b_2 & (\sigma \geq \sigma_{\text{fatigue limit}}) \end{cases} \tag{2}$$

where m_1, m_2, b_1, and b_2 are four constants determined by the linear regression of the thermal data.

The next step is to estimate the *S-N* curve, and for this Risitano [26] proposed that the total energy dissipated is constant and independent of the load applied. This energy can be estimated directly proportional to the area under the ΔT-N curve. As stage 2 is predominant in the test, the calculation of the area can be simplified as the product of the stabilized temperature in stage 2 multiplied by the number of cycles before breakage N_f:

$$\Delta T\cdot N_f = \text{constant} = \Phi \tag{3}$$

Montesano [28] reached a similar conclusion for CFRP woven laminates but obtained a better estimation with a slight modification. The thermographic data in CFRP did not show a linear relationship between ΔT and N_f, but with the ΔT and the $\log(N_f)$. The proposed model is:

$$\Delta T\cdot\log(N_f) = \text{constant} = \Phi \tag{4}$$

Finally, Huang [29] used a damage parameter to correlate the degradation of the mechanical properties of the laminate with the temperature. In his research, the normalized stiffness degradation $k(N)$ is associated with the stable temperature rise as follows:

$$k(N) = 1 - p\cdot\Delta T\cdot N^{1/q} \quad (q \geq 1) \tag{5}$$

where p and q are empirically calibrated constants. Reorganizing Eq. (5), and estimating that the degradation at the last cycle is constant and independent of the applied load [41], authors arrived to:

$$\Delta T \cdot N_f^{1/q} = \frac{1 - k(N_f)}{p} = \text{constant} = \Phi \quad (6)$$

This equation is in a similar form compared to the ones of Risitano (Eq. (3)) and Montesano (Eq. (4)), and through the relationship between ΔT and σ in Eq. (2) is possible to estimate the *S-N* curves using this methodology. Since the dissipated energy and, therefore, the measured temperature depends on factors such as the geometry and size of the specimen, the constants of Eqs. (3), (4), and (6) must be calculated for each type of sample separately.

4. Results

4.1. Static tests

The results obtained in the static test are shown in Fig. 8 where the linear elastic behavior of the material is observed. Three specimens without defects and three with defects were used. After analyzing the results of the static tests, an ultimate tensile load (UTS) of 68.1 ± 0.1 kN was obtained for the batch of defect-free specimens (A), and 57.2 ± 2 kN for the batch with defects (B). The presence of defects slightly increased the variability of the results and reduced the material strength by up to 16%. The corresponding ultimate tensile stresses are 1135 MPa for defect-free specimens (A) and 953.3 MPa for samples with defects (B).

In both cases, delamination is evident throughout the specimen, as the cracks have propagated. However, in laminates with defects, the rupture of the layers is distributed along the laminate, whereas in defect-free specimens, the rupture is concentrated at the ends. This occurs because the multiple defects at different heights and positions along the specimen cause the layers to break where the stresses are most critical due to stress concentrations. Due to the location of these undulations, the final rupture shows a stepwise pattern, with the defect in the center of the specimen being near the surface and the rest located deeper through the thickness. Notably, all waviness regions exhibited similar levels of damage, regardless of their position relative to the tabs. This clearly shows the distribution of rupture caused by the presence of defects. On the other hand, defect-free specimens do not show this pattern. As stress concentrators due to undulations are not present, the most critical areas are the ends where the defect-free specimens are clamped by the grips. This difference is shown in Fig. 9.

4.2. Fatigue tests: Estimation of fatigue limit using S-N curves

The *S-N* curves for the defect-free specimens and specimens with defects are shown in Fig. 10(a) and (b), respectively. Five specimens without defects and six with defects were tested. Due to the limited number of specimens tested, the results should be considered preliminary. The fatigue limit was established as the stress at which the laminate withstands $2 \cdot 10^6$ cycles without reaching ultimate failure. For the defect-free samples, Fig. 10(a), the fatigue limit is 742.1 ± 32.2 MPa, corresponding to a load of 44.5 ± 1.9 kN, 65% of the UTS. In these graphs, a horizontal band indicating the material failure limit under quasi-static conditions has been shaded for stresses above this limit.

For the laminate with multiple undulations as defects, Fig. 10(b), the fatigue limit is 457.2 ± 85.9 MPa, corresponding to a load of 27.4 ± 5.2 kN, which is 48% of the UTS obtained with the defective laminates. The data indicates that the presence of defects reduces the fatigue limit by almost 40% compared to the fatigue limit of the defect-free laminate. Also, the dispersion of the results obtained with the specimens with defects is almost 3 times higher. Note that the reduction of the fatigue limit with respect to the ultimate load is greater for the specimens with defects: the respective fatigue limits are 65% $UTS^{\text{defect-free}}$ and 48% $UTS^{\text{with defects}}$.

Fig. 11 displays an image captured from a specimen with defects during the tests. The presence of cracks and delaminations near the wave area, which acts as a stress concentrator, can be observed. Fig. 12(a) presents a specimen without initial defects and Fig. 12(b) one with defects, both after the final fatigue failure. Similar to the static tests, delamination is observed along the length of the laminate for the defect-free specimens, and fracture occurs near the end. Conversely, specimens with defects show a staggered fracture, prompted by the out-of-plane positioning of the waviness. Again, as discussed in the previous section, all waviness regions exhibited similar levels of damage, regardless of their position relative to the tabs. The presence of an undulation fully or partially beneath the tab did not lead to premature failure, as failure remained distributed across all defect locations.

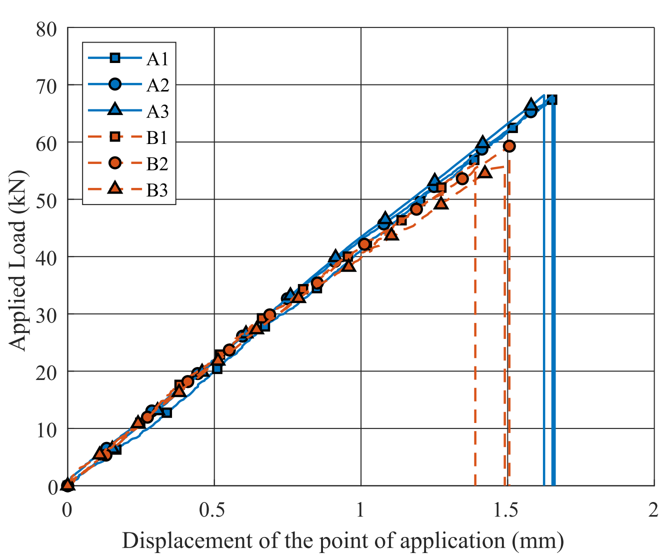

Fig. 8. Static test results: A without defects, B with defects.

4.3. Fatigue tests: Estimation of fatigue limit using thermography

Fig. 13 shows the temperature increase curves for one specimen under different loads, establishing load blocks of 7000 cycles. Two specimens without defects and two with defects were used for these tests. Given the limited number of specimens tested, the results should be considered as preliminary, providing an exploratory insight into the fatigue characterization of laminates. The temperature increment is relative to the average surface temperature of the reference specimen. The temperature used in this study is the average surface temperature of the specimen following the methodology of previous studies [23,30]. In specimens with defects, this means that the hot spots caused by the defects are averaged with the surrounding areas, but their influence remains noticeable in the overall temperature measurement. The specimen undergoes a greater temperature variation with each load increase. In general, the temperature increase *(ΔT)* stabilizes after 3500 cycles until the end of the 7000 cycles. For the lower loads, note that ΔT tends to be greater for the specimen with defects due to the effect of strain concentration at undulations.

Fig. 14 shows the results obtained from the block testing methodology, by which ΔT at the stabilized region is plotted versus the applied load. The intersection point of the two lines corresponds to the fatigue limit obtained in a test. The fatigue limit lines were estimated using the average ΔT values obtained from various specimens after repeating this procedure. The fatigue limits for the defect-free and defective laminates is 728.2 MPa and 400.3 MPa, respectively.

When comparing the thermography-based estimated value for the defect-free specimens with the fatigue limit obtained in the previous section, Fig. 10(a), the error is just 1.9%. For the laminate with defects, the error is 12.5%. Despite this higher error, it should be noted that there is a greater dispersion of results for the specimens with defects, the error falling within acceptable limits for the typical dispersion of a traditional *S-N* curve.

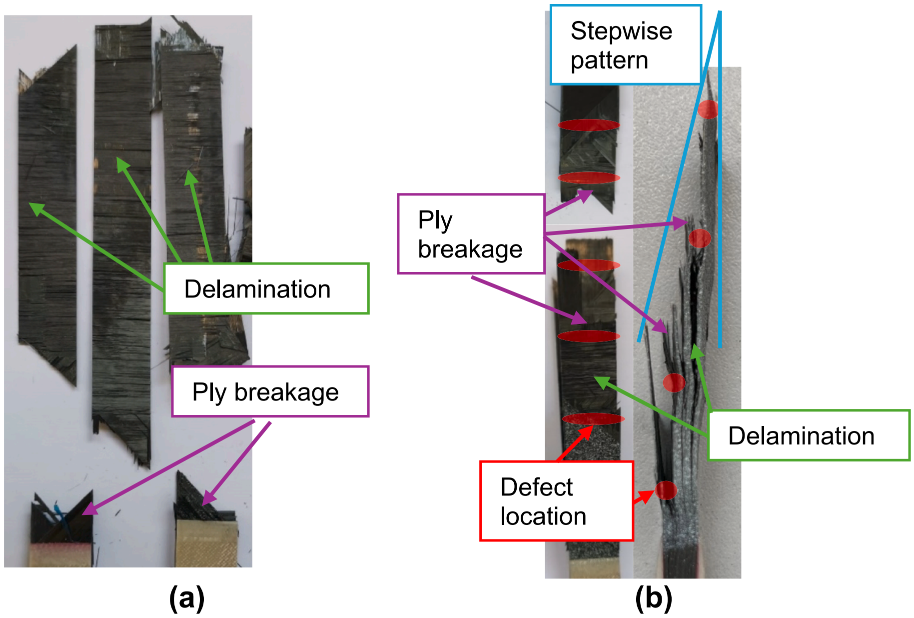

Fig. 9. Specimen after failure: (a) defect-free specimen and (b) with undulations (defects).

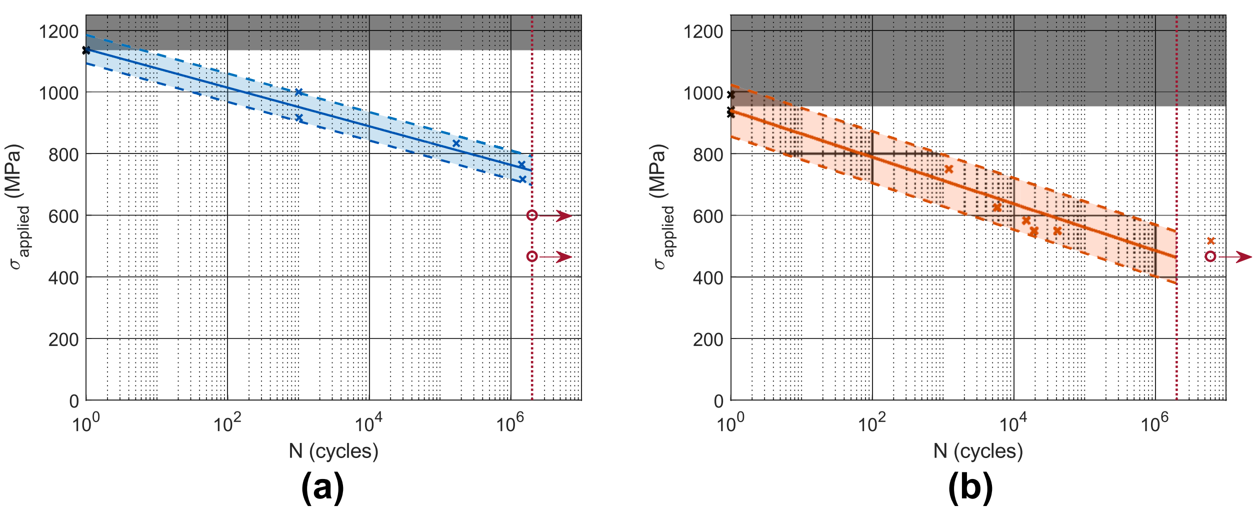

Fig. 10. *S-N* curve for (a) a defect-free specimen and (b) a specimen with undulations (defects).

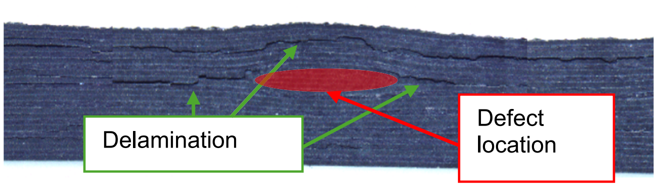

Fig. 11. Failure mechanisms surrounding the defect observed after fatigue testing.

4.4. Fatigue tests: Estimation of S-N curves using thermographic methodology

From the regressions shown in Fig. 14, the parameters for Eq. (2) in defect-free and defective specimens are calibrated for $\Delta T^{\text{defect-free}}(\sigma)$ and $\Delta T^{\text{with defects}}(\sigma)$. After that, the constant of Eq. (3) (Risitano), Eq. (4) (Montesano) and the constant and q of Eq. (6) (Huang) are calculated. To this aim, the data from Fig. 10 were used, and the value of each constant is shown in Tables 1 (defect-free) and 2 (with defects). The parameters of the Huang method have been fit by least squares for all the specimens of each case:

From the data in Tables 1 and 2, it can be observed that the results obtained using Risitano's method are much less accurate. This confirms the nonlinearity of the relationship between ΔT and σ as discussed by Montesano, whereas the results obtained with the Montesano's logarithmic method fit much better. This is evident in Fig. 15, which shows the poor fit achieved with Risitano's model. On the other hand, both the Huang and Montesano models show similar trends. The Huang's model seems to fit better at low cycles, although this region is heavily dominated by static failure so either model could be used. This analysis shows that the *S-N* curve obtained through thermography fits well for both defect-free and defective specimens. This demonstrates the applicability of this methodology as a useful tool in the fatigue characterization of laminates with defects.

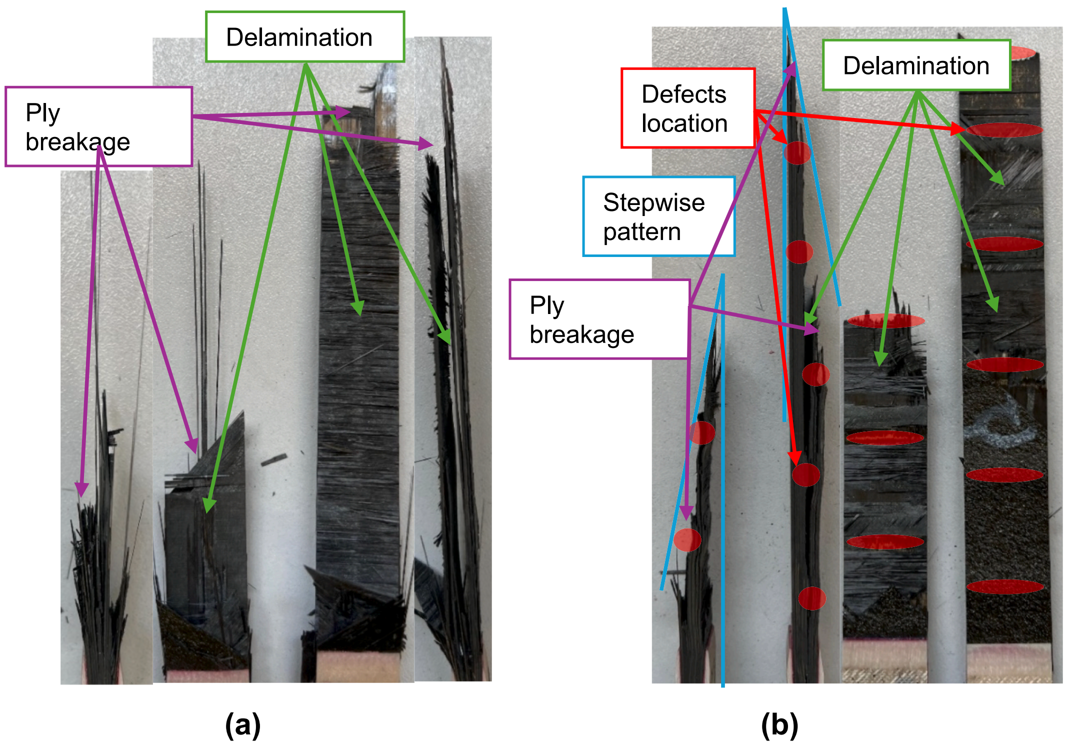

Fig. 12. Specimen after fatigue: (a) defect-free and (b) with defects.

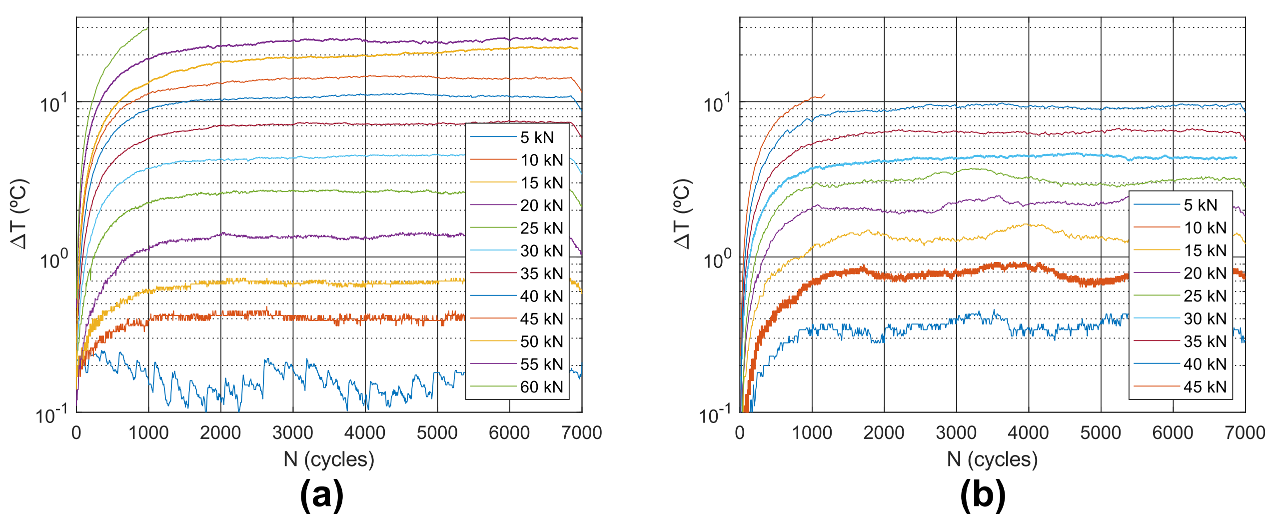

Fig. 13. Examples of ΔT-N curves for a defect-free specimen (a) and a specimen with defects (b).

4.5. Fatigue tests: Defect location

In addition to characterizing the fatigue behavior of laminates, both with and without defects, thermal images are useful for locating these defects in the component. Fig. 16 shows two thermal images obtained at a load of 45 kN after 50 cycles: the specimen with defects is shown on the left; the defect-free specimen on the right. It can be seen how the thermal camera captures the location of defects in the specimen with waviness. The temperature in the affected area is around 2°C higher than the average temperature between defects. However, it should be emphasized that this increase can go unnoticed at low loads as the temperature increment will be below the thermal camera sensitivity. Defects can also be challenging to locate if they are near the load application zones, such as those close to the machine grips marked in the image with red arrows.

5. Conclusions

In this study, we validated various models for analyzing fatigue behavior and characterizing the fatigue limit of CFRP composite materials with multiple undulation defects using infrared thermography. This approach represents a significant advance over previous research, as it addresses the challenges due to the presence of defects and provides a reliable estimation of fatigue performance under practical conditions. The main results of the study are summarized as follows:

1. It has been confirmed that the undulation defects generated during the manufacturing of CFRP laminates significantly reduce the material tensile strength (up to 16%) and considerably decrease its fatigue life up to 40%. This underscores the need to detect and characterize this type of defects.

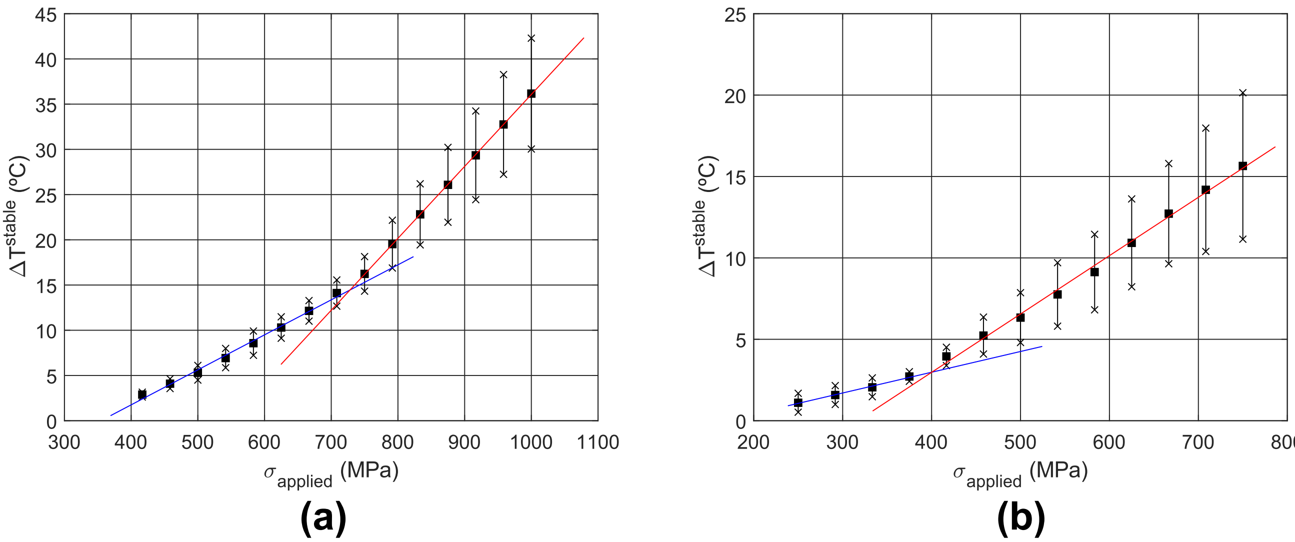

Fig. 14. Examples of ΔT-S curves obtained for a defect-free specimen (a) and a specimen with defects (b).

Table 1
Constants calculation for thermographic methods with defect-free specimens.

	N_f (Cycles)	$\sigma_{applied}$ (MPa)	$\Delta T^{defect-free}$ (°C)	$\Phi^{Risitano}$	$\Phi^{Montesano}$	Φ^{Huang}	q^{Huang}
A4	1010	1000	35.49	35847	107	62.3	10.6
A5	1021	917	28.95	29956	87		
A6	169971	833	22.41	$3.81\cdot10^6$	117		
A7	$1.42\cdot10^6$	765	17.02	$24.26\cdot10^6$	104		
A8	$1.47\cdot10^6$	717	13.63	$20.04\cdot10^6$	84		
			Mean:	$9.63\cdot10^6$	99.96		

Table 2
Constants calculation for thermographic methods with defective specimens.

	N_f (Cycles)	$\sigma_{applied}$ (MPa)	$\Delta T^{with\ defects}$ (°C)	$\Phi^{Risitano}$	$\Phi^{Montesano}$	Φ^{Huang}	q^{Huang}
B4	1202	750	14.64	17600	45	29.9	8.5
B5	5807	625.5	10.47	60780	39		
B6	15100	583	9.05	136710	38		
B7	19463	550	7.94	154470	34		
B8	41288	550	7.94	327680	37		
B9	$6.09\cdot10^6$	517	6.82	$41.55\cdot10^6$	46		
			Mean:	$7.04\cdot10^6$	39.88		

2. Furthermore, the results demonstrate that thermographic methods can be used to establish methodologies for predicting the fatigue limit of CFRP laminates, both in the presence of defects and without them. This significantly reduces the cost and time required for traditional testing to obtain the fatigue limit for the material. In this work, the errors in this procedure did not exceed 12.5% in the most unfavorable case, which is deemed acceptable. This demonstrates that thermography enables the rapid and straightforward fatigue characterization of CFRP laminates even in the presence of defects.
3. With the methodologies developed to date, thermography allows the estimation of the *S-N* curve. The results confirm that Risitano's method is significantly less accurate, supporting the nonlinearity of the ΔT-σ relationship discussed by Montesano, whereas Montesano's logarithmic method provides a much better fit. Both Huang and Montesano models show similar trends, with Huang's model fitting better at low cycles, although static failure dominates this region, making either model viable. The *S-N* curves obtained through thermography are valid for both defect-free and defective specimens.
4. The application of infrared thermography to a component in service also allows the localization of a local defect. The defect should be located away from the load application area, as this area will be affected by a greater temperature increase, which may hinder the correct localization of the waviness.
5. The results obtained in this study are highly promising, demonstrating the feasibility of infrared thermography for the rapid and accurate characterization of the fatigue limit in CFRP laminates, even in the presence of complex waviness defects. However, it is important to note that the number of specimens tested is limited. Expanding the experimentation is recommended to validate and strengthen the findings. Despite this limitation, this work represents a valuable exploratory study of the application of thermography as a non-destructive inspection and characterization tool.

CRediT authorship contribution statement

José Vicente Calvo: Writing – original draft, Visualization,

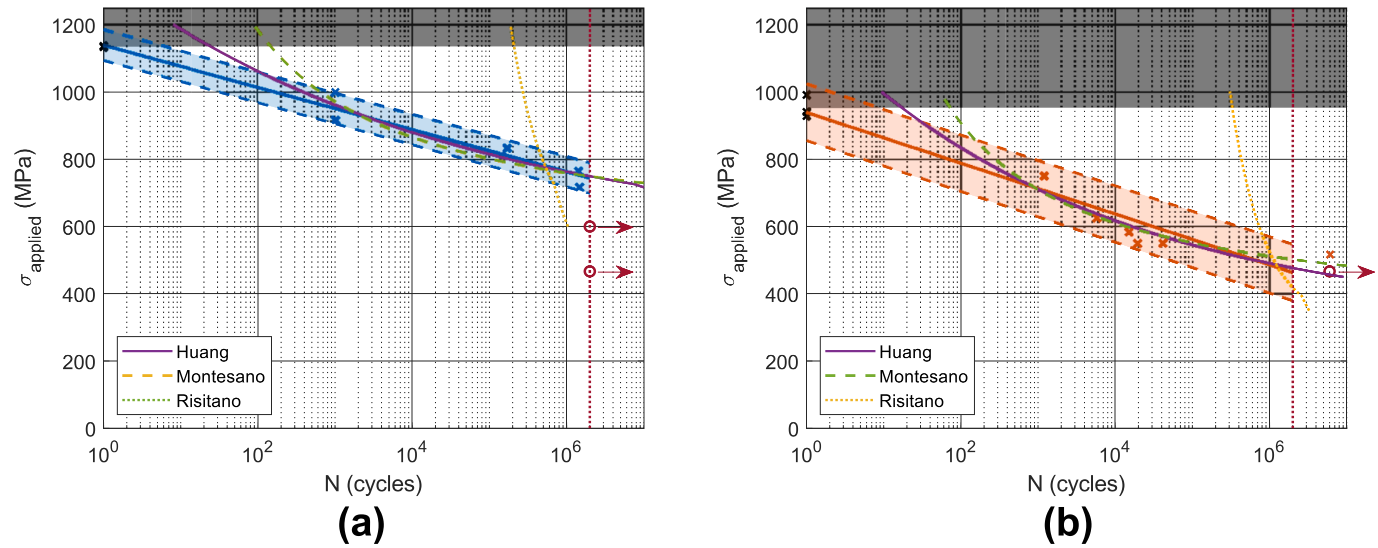

Fig. 15. *S-N* curve for a defect-free specimen (a) and a specimen with waving defects (b) including curves estimated through thermographic methodologies.

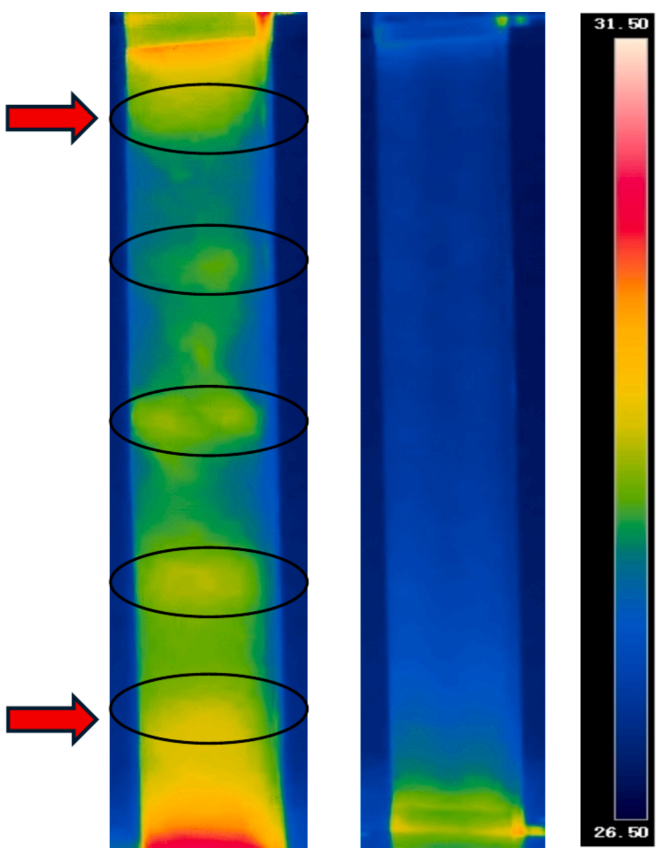

Fig. 16. Defect localization using thermal images. Left: with defects, right: without defects.

Validation, Software, Methodology, Investigation, Formal analysis, Data curation, Conceptualization. **Norberto Feito:** Writing – review & editing, Visualization, Supervision, Resources, Funding acquisition. **Eugenio Giner:** Writing – review & editing, Supervision, Resources, Project administration, Funding acquisition, Conceptualization.

Funding

This research is part of the R+D+i project PID2023-151610OB-C22, funded by MCIN/AEI/10.13039/501100011033 and by "ERDF: A way of making Europe". Grant PRE2018-086277 funded by MCIN/AEI/10.13039/501100011033 and by "ESF Investing in your future". The funding of the Generalitat Valenciana, Programme PROMETEO 2021/046, and project GV/2021/060, is also acknowledged.

Declaration of competing interest

The authors declare that they have no known competing financial interests or personal relationships that could have appeared to influence the work reported in this paper.

Data availability

Data will be made available on request.

References

[1] Potter K, Khan B, Wisnom M, Bell T, Stevens J. Variability, fibre waviness and misalignment in the determination of the properties of composite materials and structures. Compos Part Appl Sci Manuf 2008;39:1343–54. https://doi.org/10.1016/j.compositesa.2008.04.016.

[2] Kulkarni P, Mali KD, Singh S. An overview of the formation of fibre waviness and its effect on the mechanical performance of fibre reinforced polymer composites. Compos Part Appl Sci Manuf 2020;137:106013. https://doi.org/10.1016/j.compositesa.2020.106013.

[3] Hassan MH, Othman AR, Kamaruddin S. A review on the manufacturing defects of complex-shaped laminate in aircraft composite structures. Int J Adv Manuf Technol 2017;91:4081–94. https://doi.org/10.1007/s00170-017-0096-5.

[4] Lerman MW, Cairns DS, Nelson JW. Investigation of the effect of in-plane fiber waviness in composite materials through multiple scales of testing and finite element modeling. Sandia National Lab. (SNL-NM), Albuquerque, NM (United States); Sandia National Lab. (SNL-CA), Livermore, CA (United States), 2015. https://doi.org/10.2172/1505394.

[5] Pandey RK, Sun CT. Mechanisms of wrinkle formation during the processing of composite laminates. Compos Sci Technol 1999;59:405–17. https://doi.org/10.1016/S0266-3538(98)00080-3.

[6] Potter KD, Campbell M, Langer C, Wisnom MR. The generation of geometrical deformations due to tool/part interaction in the manufacture of composite components. Compos Part Appl Sci Manuf 2005;36:301–8. https://doi.org/10.1016/j.compositesa.2004.06.002.

[7] Hallander P, Akermo M, Mattei C, Petersson M, Nyman T. An experimental study of mechanisms behind wrinkle development during forming of composite laminates. Compos Part Appl Sci Manuf 2013;50:54–64. https://doi.org/10.1016/j.compositesa.2013.03.013.

[8] Potter K. Understanding the origins of defects and variability in composites manufacture. ICCM int conf compos mater. 2009.

[9] Beakou A, Cano M, Le Cam J-B, Verney V. Modelling slit tape buckling during automated prepreg manufacturing: a local approach. Compos Struct 2011;93:2628–35. https://doi.org/10.1016/j.compstruct.2011.04.030.

[10] Belnoue J-P-H, Mesogitis T, Nixon-Pearson OJ, Kratz J, Ivanov DS, Partridge IK, et al. Understanding and predicting defect formation in automated fibre placement pre-preg laminates. Compos Part Appl Sci Manuf 2017;102:196–206. https://doi.org/10.1016/j.compositesa.2017.08.008.
[11] Stamopoulos AG, Ilio AD. On the predictive tools for assessing the effect of manufacturing defects on the mechanical properties of composite materials. Procedia CIRP 2019;79:563–7. https://doi.org/10.1016/j.procir.2019.02.108.
[12] Bogetti TA, Gillespie JW, Lamontia MA. Influence of ply waviness on the stiffness and strength reduction on composite laminates. J Thermoplast Compos Mater 1992;5:344–69. https://doi.org/10.1177/089270579200500405.
[13] Chan WS, Wang JS. Influence of fiber waviness on the structural response of composite laminates. J Thermoplast Compos Mater 1994;7:243–60. https://doi.org/10.1177/089270579400700306.
[14] Hsiao HM, Daniel IM. Elastic properties of composites with fiber waviness. Compos Part Appl Sci Manuf 1996;27:931–41. https://doi.org/10.1016/1359-835X(96)00034-6.
[15] Zhu J, Wang J, Zu L. Influence of out-of-plane ply waviness on elastic properties of composite laminates under uniaxial loading. Compos Struct 2015;132:440–50. https://doi.org/10.1016/j.compstruct.2015.05.062.
[16] Takeda T. Micromechanics model for three-dimensional effective elastic properties of composite laminates with ply wrinkles. Compos Struct 2018;189:419–27. https://doi.org/10.1016/j.compstruct.2017.10.086.
[17] Altmann A, Gesell P, Drechsler K. Strength prediction of ply waviness in composite materials considering matrix dominated effects. Compos Struct 2015;127:51–9. https://doi.org/10.1016/j.compstruct.2015.02.024.
[18] Mukhopadhyay S, Jones MI, Hallett SR. Tensile failure of laminates containing an embedded wrinkle; numerical and experimental study. Compos Part Appl Sci Manuf 2015;77:219–28. https://doi.org/10.1016/j.compositesa.2015.07.007.
[19] Mukhopadhyay S, Nixon-Pearson OJ, Hallett SR. An experimental and numerical study on fatigue damage development in laminates containing embedded wrinkle defects. Int J Fatigue 2018;107:1–12. https://doi.org/10.1016/j.ijfatigue.2017.10.008.
[20] Nikishkov Y, Makeev A, Seon G. Progressive fatigue damage simulation method for composites. Int J Fatigue 2013;48:266–79. https://doi.org/10.1016/j.ijfatigue.2012.11.005.
[21] May M, Hallett SR. A combined model for initiation and propagation of damage under fatigue loading for cohesive interface elements. Compos Part Appl Sci Manuf 2010;41:1787–96. https://doi.org/10.1016/j.compositesa.2010.08.015.
[22] Calvo JV, Quiñonero-Moya AR, Feito N, Miguélez MH, Giner E. Influence of distributed out-of-plane waviness defects on the mechanical behavior of CFRP laminates. Compos Struct 2023;323:117498. https://doi.org/10.1016/j.compstruct.2023.117498.
[23] Toubal L, Karama M, Lorrain B. Damage evolution and infrared thermography in woven composite laminates under fatigue loading. Int J Fatigue 2006;28:1867–72. https://doi.org/10.1016/j.ijfatigue.2006.01.013.
[24] Feito N, Calvo JV, Belda R, Giner E. An experimental and numerical investigation to characterize an aerospace composite material with open-hole using non-destructive techniques. Sensors 2020;20:4148. https://doi.org/10.3390/s20154148.
[25] La Rosa G, Risitano A. Thermographic methodology for rapid determination of the fatigue limit of materials and mechanical components. Int J Fatigue 2000;22:65–73. https://doi.org/10.1016/S0142-1123(99)00088-2.
[26] Fargione G, Geraci A, La Rosa G, Risitano A. Rapid determination of the fatigue curve by the thermographic method. Int J Fatigue 2002;24:11–9. https://doi.org/10.1016/S0142-1123(01)00107-4.
[27] Colombo C, Libonati F, Pezzani F, Salerno A, Vergani L. Fatigue behaviour of a GFRP laminate by thermographic measurements. Procedia Eng 2011;10:3518–27. https://doi.org/10.1016/j.proeng.2011.04.579.
[28] Montesano J, Fawaz Z, Bougherara H. Use of infrared thermography to investigate the fatigue behavior of a carbon fiber reinforced polymer composite. Compos Struct 2013;97:76–83. https://doi.org/10.1016/j.compstruct.2012.09.046.
[29] Huang J, Pastor ML, Garnier C, Gong XJ. A new model for fatigue life prediction based on infrared thermography and degradation process for CFRP composite laminates. Int J Fatigue 2019;120:87–95. https://doi.org/10.1016/j.ijfatigue.2018.11.002.
[30] Yu F, Zhou B, Xin W, Zhang X. Fatigue life prediction for the main spar with wrinkle defects of a wind turbine blade. Fatigue Fract Eng Mater Struct 2021;44:2764–80. https://doi.org/10.1111/ffe.13545.
[31] An B, Li A, Mao Q, Huang J. Investigating the relationship between fracture entropy and stress amplitude in CFRP laminates under low-cycle fatigue loading. Thin-Walled Struct 2024;202:112040. https://doi.org/10.1016/j.tws.2024.112040.
[32] Gamstedt EK, Talreja R. Fatigue damage mechanisms in unidirectional carbon-fibre-reinforced plastics. J Mater Sci 1999;34:2535–46. https://doi.org/10.1023/A:1004684228765.
[33] Boulanger T, Chrysochoos A, Mabru C, Galtier A. Calorimetric analysis of dissipative and thermoelastic effects associated with the fatigue behavior of steels. Int J Fatigue 2004;26:221–9. https://doi.org/10.1016/S0142-1123(03)00171-3.
[34] Giancane S, Chrysochoos A, Dattoma V, Wattrisse B. Deformation and dissipated energies for high cycle fatigue of 2024-T3 aluminium alloy. Theor Appl Fract Mech 2009;52:117–21. https://doi.org/10.1016/j.tafmec.2009.08.004.
[35] Guo Q, Guo X, Fan J, Syed R, Wu C. An energy method for rapid evaluation of high-cycle fatigue parameters based on intrinsic dissipation. Int J Fatigue 2015;80:136–44. https://doi.org/10.1016/j.ijfatigue.2015.04.016.
[36] Guo Q, Guo X. Research on high-cycle fatigue behavior of FV520B stainless steel based on intrinsic dissipation. Mater Des 2016;90:248–55. https://doi.org/10.1016/j.matdes.2015.10.103.
[37] Huang J, Pastor M-L, Garnier C, Gong X. Rapid evaluation of fatigue limit on thermographic data analysis. Int J Fatigue 2017;104:293–301. https://doi.org/10.1016/j.ijfatigue.2017.07.029.
[38] Wang XG, Crupi V, Guo XL, Zhao YG. Quantitative Thermographic Methodology for fatigue assessment and stress measurement. Int J Fatigue 2010;32:1970–6. https://doi.org/10.1016/j.ijfatigue.2010.07.004.
[39] Luong MP. Infrared thermographic scanning of fatigue in metals. Nucl Eng Des 1995;158:363–76. https://doi.org/10.1016/0029-5493(95)01043-H.
[40] Luong MP. Fatigue limit evaluation of metals using an infrared thermographic technique. Mech Mater 1998;28:155–63. https://doi.org/10.1016/S0167-6636(97)00047-1.
[41] Peng T, Liu Y, Saxena A, Goebel K. In-situ fatigue life prognosis for composite laminates based on stiffness degradation. Compos Struct 2015;132:155–65. https://doi.org/10.1016/j.compstruct.2015.05.006.